GMR
The Original

SOLUTION PROCESSED SNO_2–TIO_2 HETEROJUNCTION NANOCOMPOSITES FOR ENHANCED PHOTOCATALYTIC DEGRADATION AND ELECTROCHEMICAL ENERGY STORAGE APPLICATIONS

K. Parivathini[1], E. Tamil Selvi[2], M.E. Rajasaravanan[3], P. Matheswaran[4*]

[1]Department of Physics, Tagore Institute of Engineering and Technology, Deviyakurichi- 636 112, Tamilnadu, India
[2]Department of Physics, Annapoorna Engineering College(A), Salem 636308, Tamilnadu, India
[3]Department of Physics, Govt. Arts College(A), Salem 636007, Tamilnadu, India
[4*]Department of Chemistry, Govt. Arts College(A), Salem 636007, Tamilnadu, India, email id: matheshkutty77@gmail.com

ABSTRACT
The unique properties of heterojunction nanocomposites, including enhanced charge separation, superior photocatalytic activity, and improved electrochemical performance, have attracted significant attention for environmental remediation and energy storage applications. In this study, a SnO_2-doped TiO_2 nanocomposite was successfully synthesized via a simple solution-based method. The structural and phase characteristics of the synthesized nanocomposite were investigated using X-ray diffraction (XRD) and Raman spectroscopy, while the morphology and microstructure were examined by transmission electron microscopy (TEM). The photocatalytic activity was evaluated using methylene blue (MB) as a model organic dye under UV irradiation. In addition, the electrochemical performance of the nanocomposite was systematically investigated by cyclic voltammetry (CV) and electrochemical impedance spectroscopy (EIS) to assess its charge storage capability and charge-transfer characteristics. The SnO_2-doped TiO_2 nanocomposite exhibited excellent photocatalytic efficiency, achieving 94% degradation of MB within 120 min. The enhanced photocatalytic and electrochemical performances are attributed to the formation of an effective SnO_2/TiO_2 heterojunction, which promotes efficient separation and transport of photogenerated electron–hole pairs, reduces charge recombination, and lowers the interfacial charge-transfer resistance, as confirmed by the EIS analysis. These findings demonstrate that the SnO_2-doped TiO_2 nanocomposite is a promising multifunctional material for both photocatalytic pollutant degradation and electrochemical energy storage applications.

KEYWORDS: SnO2 nanocomposite; Sol-gel method; Photocatalytic activity; Methylene blue dye

INTRODUCTION
Eco-friendly environments are seriously threatened by the terrible pollution that is being caused by the rapid processes of industrialization and civilization. Water pollution is one of the main concerns when it comes to different forms of pollution. It not only has detrimental effects on health but also changes how aquatic organisms live. Consequently, the number of preventable deaths brought on by water contamination is rising daily. Because organic contaminants from the textile, food, paint, and leather industries often contaminate water supplies, recycling or purifying their waste is a difficult undertaking [1-4]. The development of quick, highly effective, and inexpensive processes for physically, chemically, and biologically breaking down these contaminants is of great interest to research communities. Solar-driven semiconductor-based photocatalysis technology is one of these techniques that has drawn a lot of interest since it is easy to use, environmentally friendly, and can break down organic pollutants without producing any byproducts [5-7]. A variety of semiconductor materials, such as metal oxides [8–11], transition metal sulfides [12–15], carbon-based materials [16–19], and metal-organic frameworks (MOFs), have been employed for photocatalysis. Since metal oxides have a large binding energy for excitons, a wide bandgap, low toxicity, and excellent chemical stability, they have been studied in the field of photocatalysis extensively.
Unfortunately, the actual applicability of semiconductor metal oxides is limited because most of them only absorb UV light. In order to get over this restriction, researchers have looked into combining two metal oxides to cover the UV and visible spectrums, which will improve the photocatalytic characteristics. Among these mixes, it has been discovered that a nanocomposite of SnO2 and TiO2 forms an n-p junction, improving its photocatalytic capabilities. This is explained by the huge bandgap of SnO2 and TiO2, their non-toxic nature, high photosensitivity, and low recombination rate. TiO2 is a p-type semiconductor (1.5 eV) while SnO2 is a broad bandgap n-type semiconductor (3.7 eV). Since TiO2 functions as a sink in the n-p heterojunction, it helps to keep electron-hole pairs apart and permits photogenerated electrons and holes to go in opposing directions. As a result, electrons build up in SnO2's valence band, which lowers the rate at which electron-hole couples recombine. The SnO2 doped TiO2 nanocomposite has better photocatalytic capabilities overall because of its minimal recombination, or high electron movement in the opposite direction [20-23]. This study used a straightforward solution-based technique to synthesis a TiO2 nanocomposite photocatalyst doped with SnO2. Using XRD, UV-Vis,

Raman spectroscopy, and TEM examination, the catalyst's structural, optical, and morphological properties were carefully examined. The degradation of MB dye under UV light illumination was used to measure the photocatalytic activity of the catalyst. Additionally, a thorough investigation was conducted into the catalyst's photocatalytic activities for the breakdown of highly concentrated malachite green dyes.

2. Experimental section

2.1. Materials

Titanium dioxide (TiO2), tin chloride pentahydrate (SnCl4.5H2O), sodium hydroxide (NaOH),Polyvinylpyrrolidone (PVP), Ethanol (C2H5OH) were purchased from Sisco Research Laboratories Pvt. Ltd. (SRL) - India. All the chemicals were used without further purification.

2.2. Preparation of SnO2 doped TiO2

A straightforward solution processing technique was utilized to successfully synthesis a nanocomposite photocatalyst made of SnO2-doped TiO2. The following steps were included in the synthesis process: First, 100 mL of deionized (DI) water was mixed with a 1:1 ratio of TiO2 and tin chloride pentahydrate, and the mixture was agitated for an hour. The clear solution was then combined with 0.1 g of PVP and swirled for duration of 15 minutes. Next, 50 milliliters of water were used to dissolve 1.5 grams of sodium hydroxide, and this sodium hydroxide solution was progressively added to the previously obtained homogenous solution. The resultant precipitate was gathered and repeatedly cleaned with ethanol and DI water. In the end, the product was air-cooled for three hours at 400°C and dried for an entire night at 80°C. The substance that was synthesized was identified as SnO2/TiO2. In order to provide a comparison, distinct synthesis procedures were carried out under the previously specified reaction conditions to produce SnO2 and TiO2 without the addition of copper acetate tetrahydrate and tin chloride pentahydrate, respectively.

2.3 Characterization Techniques

The crystalline structure of the synthesized SnO_2–TiO_2 nanocomposite was analyzed using an X-ray diffractometer (AERIS high-resolution benchtop) with Cu Kα radiation (λ = 1.5406 Å). The morphology, microstructure, and elemental composition were examined using high-resolution transmission electron microscopy (HR-TEM, JEOL JEM-2100 Plus, Japan) operated at 200 kV and high-resolution scanning electron microscopy (HR-SEM, Thermo Scientific Apreo S) equipped with energy-dispersive X-ray spectroscopy (EDX). Raman spectra were recorded using a HORIBA LABRAM HR Evolution Raman spectrometer with a 532 nm excitation laser to investigate the vibrational characteristics of the synthesized materials. The optical properties were evaluated using a UV–Vis diffuse reflectance spectrophotometer (SHIMADZU UV-3600 Plus). The electrochemical behavior of the SnO_2–TiO_2 nanocomposite was investigated using a SquadStat Plus electrochemical workstation (Admiral Instruments) through cyclic voltammetry (CV) and electrochemical impedance spectroscopy (EIS) measurements in a three-electrode configuration, employing Ag/AgCl as the reference electrode, a platinum wire as the counter electrode, and the coated sample as the working electrode in 1 M KOH aqueous electrolyte.

2.4. Photocatalyticdye degradation test

The degradation of an organic pollutant under ultraviolet (UV) light was used to test the photocatalytic capabilities of a synthetic nanocomposite catalyst made of TiO2 doped with SnO2. A solution containing 10 ppm of methylene blue (MB) dye was made in a conventional degradation procedure by mixing it with 50 mL of deionized (DI) water and stirring for 15 minutes. The aforementioned solution was then mixed with 50 mg of the SnO2 doped TiO2 nanocomposite catalyst and left to stir for 20 minutes in a dark setting. Subsequently, the catalyst and model pollutant mixture was put at a distance of 10 cm from the solution's surface and exposed to UV radiation. The organic pollutant-containing solution was gathered every 30 minutes, and the UV-Visible absorption spectrum was analyzed. The decomposition rate of each catalyst was determined using the equation provided [24].

$$\text{Dye degradation efficiency (\%)} = \frac{C_0 - C_t}{C_0} \times 100$$

where, C0= initial concentration and Ct is reaction concentration at time t, respectively.

3. RESULTS AND DISCUSSION

3.1. XRD analyses

Different diffraction peaks at angles of 25.38°, 33.81°, 38.91°, 51.55°, 54.37°, and 65.61° are seen in Figure 1 for the SnO2 sample. The planes (110), (101), (200), (210), (211), (112), and (301), in that order, are responsible for these peaks. The sample and the JCPDS card no. 41-1445 both fit the tetragonal rutile structure. At angles of 32.51°, 35.55°, 38.72°, 48.75°, 53.48°, and 68.07°, respectively, the planes (110), (002), (111), (020), (202), and (220) are represented by prominent diffraction peaks in the TiO2 XRD pattern. These peaks all match the monoclinic TiO2 structure quite well. When SnO2 and TiO2 are combined, the diffraction pattern essentially stays the same, indicating the creation of a SnO2-doped TiO2 nanocomposite [25].

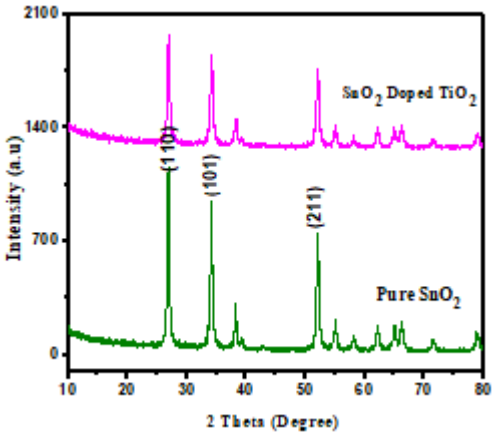

Fig. 1. XRD pattern of pure and SnO2 doped TiO2 nano material

3.2 UV-Vis analysis

We looked into the optical absorption and optical band gap characteristics of nanocomposite samples made of SnO2 and TiO2 doped with SnO2, as shown in Figure 2. These nanocomposite materials' optical absorption spectra were studied between 200 and 700 nm in wavelength. The absorption margins of pure SnO2 and TiO2 samples were found to be around 400 nm and 700 nm, respectively. But when SnO2 and TiO2 were mixed, a new absorption edge at 500 nm appeared, indicating the existence of an extra energy level within the bandgap. This change in absorption suggests that a new energy state has been introduced.

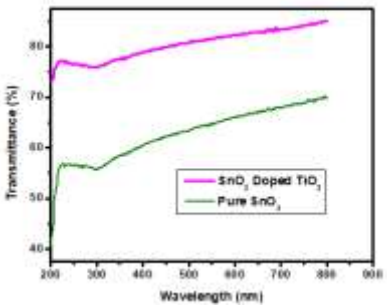

Fig. 2. UV-Vis Transmittance spectrum of pure and SnO2 doped TiO2 nano material

The Kubelka-Munk method has been utilized to calculate the energy band gap values. At any given wavelength, the Kubelka-Munk function is expressed as follows:

$$\frac{\alpha}{S} = F(R) = \frac{(1-R)^2}{2R} \quad (1)$$

$$R = \frac{R_{Sample}}{R_{Standard}} \quad (2)$$

where S stands for the scattering coefficient, α for the absorption coefficient, and R for reflectance. The bandgap values of the SnO2 and SnO2 doped TiO2 nanocomposite samples were found to be 3.56, 1.60, and 2.3 eV, respectively, as shown in figure 3. It is important to note that the samples' photocatalytic properties are enhanced by this rise in energy level [27].

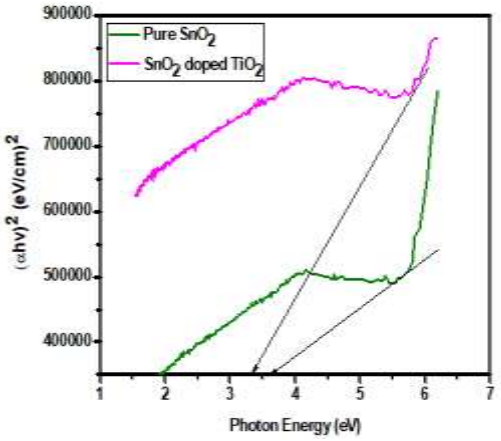

Fig. 3. Bandgap energy of pure and SnO2doped TiO2 nano material

3.3. FTIR investigation

Figure 4 illustrates the Fourier transform infrared (FT-IR) spectra of pure SnO_2 and the SnO_2-doped TiO_2 nanocomposite, which were recorded to investigate the functional groups and chemical bonding present in the synthesized materials. The FT-IR spectra confirm the successful formation of the SnO_2/TiO_2 heterostructure through the presence of characteristic vibrational bands corresponding to hydroxyl groups, residual organic species, and metal–oxygen bonds. A broad and intense absorption band centered at approximately 3433 cm^{-1} is attributed to the stretching vibration of hydroxyl (O–H) groups associated with adsorbed water molecules and surface hydroxyl species. The presence of these hydroxyl groups is beneficial for photocatalytic applications, as they can readily react with photogenerated holes to produce highly reactive hydroxyl radicals (•OH), thereby enhancing the degradation of organic pollutants. A weak absorption band observed around 1630 cm^{-1} (if present) can be assigned to the bending vibration of molecular water adsorbed on the surface of the nanocomposite.

The absorption bands located at approximately 2927 cm^{-1} and 1388 cm^{-1} correspond to the stretching vibrations of C–H and the bending vibrations associated with N–H/C–N functional groups originating from residual polyvinylpyrrolidone (PVP), which was employed as a stabilizing and capping agent during the synthesis process. The relatively low intensity of these bands indicates that most of the organic species were effectively removed during the annealing treatment, leaving only trace amounts adsorbed on the particle surface. In the lower wavenumber region, the FT-IR spectrum exhibits strong characteristic absorption bands at approximately 620 cm^{-1} and 580 cm^{-1}, which are assigned to the stretching vibrations of Sn–O and Ti–O bonds, respectively. These bands confirm the formation of crystalline SnO_2 and TiO_2 phases within the nanocomposite. The slight shift and broadening of these metal–oxygen vibrational bands compared with pure SnO_2 indicate strong interfacial interaction between SnO_2 and TiO_2, suggesting the successful formation of a heterojunction rather than a simple physical mixture of the two oxides. Furthermore, the broad absorption region extending from 700 to 400 cm^{-1} is characteristic of metal–oxygen (M–O) lattice vibrations commonly observed in metal oxide nanomaterials. The enhanced intensity of this region in the SnO_2-doped TiO_2 nanocomposite further supports the coexistence of Sn–O–Sn, Ti–O–Ti, and possible interfacial Sn–O–Ti linkages, indicating effective integration of the two semiconductor phases.

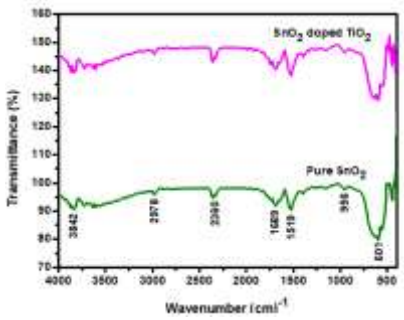

Fig. 4. FTIR spectrum of pure and SnO2doped TiO2 nano material

3.5. TEM analyses

Figure 6 presents the transmission electron microscopy (TEM) images of the synthesized SnO_2-doped TiO_2 nanocomposite. The TEM analysis reveals that the nanocomposite consists of uniformly distributed TiO_2 nanoparticles anchored onto rock-like SnO_2 structures, forming a well-integrated heterojunction architecture. The particles are closely interconnected without significant agglomeration, providing a large interfacial contact area between SnO_2 and TiO_2. Such an intimate heterostructure is beneficial for enhancing charge separation and facilitating efficient electron transport during photocatalytic and electrochemical processes. The high-resolution TEM (HR-TEM) image clearly displays well-resolved lattice fringes, confirming the highly crystalline nature of the synthesized nanocomposite. The observed lattice spacings can be assigned to the characteristic crystallographic planes of tetragonal SnO_2 and anatase TiO_2, demonstrating the successful coexistence of both phases within the heterostructure. The sharp and continuous lattice fringes indicate excellent crystallinity with minimal structural defects, which is advantageous for improving charge carrier mobility and reducing electron–hole recombination. The formation of a coherent interface between SnO_2 and TiO_2 promotes efficient interfacial charge transfer, thereby enhancing both photocatalytic degradation efficiency and electrochemical performance. The particle size observed in the TEM images is in the nanometer range, with TiO_2 nanoparticles uniformly decorating the surface of the larger SnO_2 particles. Although nanosized grains contain numerous grain boundaries that can serve as charge trapping sites, the formation of the SnO_2/TiO_2 heterojunction effectively minimizes the adverse effects of these grain boundaries by providing rapid pathways for electron migration across the interface. Consequently, photogenerated electrons can be efficiently transferred from TiO_2 to SnO_2, suppressing electron–hole recombination and increasing the lifetime of charge carriers.

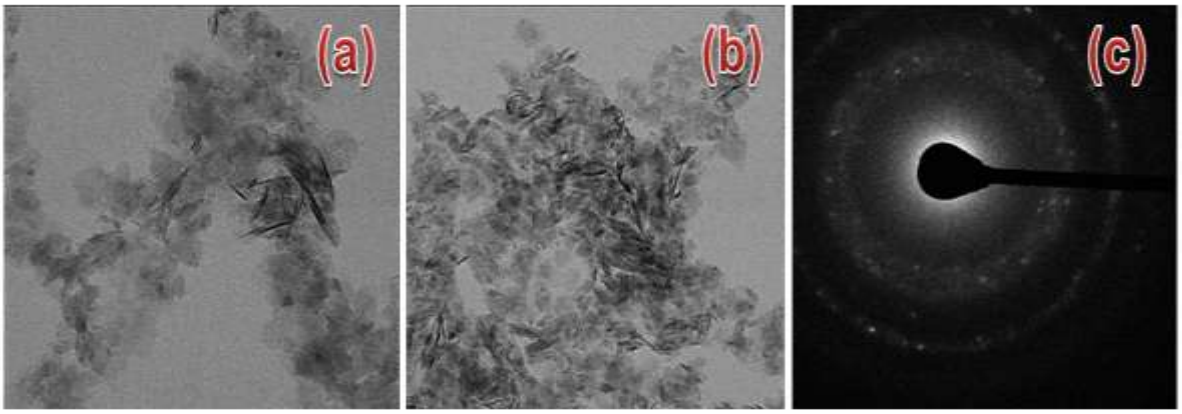

Fig. 6. (a) TEM images of pure SnO2 (b) SnO2 doped TiO2 nanocomposite (c) SAED pattern

3.6. Photocatalytic activity

Upon examination of the characteristics previously described, it was clear that the manufactured materials showed notable improvements in their absorption of visible light, a high degree of crystallinity, and effective separation properties. The decolorization of MB dye in the presence of visible light was used to gauge the photocatalytic potential of the generated samples. The absorption spectra were recorded using a UV-Vis spectrophotometer in order to evaluate the effectiveness of the photocatalysts. Every experiment involving dye degradation lasted 120 minutes, or until the contaminant was entirely eliminated.

It was possible to see that as the irradiation period grew by looking at the absorption spectra that the typical peak at 660 nm gradually decreased. The blue color in the solution completely vanished after 120 minutes, suggesting that the photodegradation process had been successful. This was due to the MB dye's complete absorption. Methylene blue (MB) concentration at a given time (t) was represented by C, whereas the initial concentration following the catalyst's adsorption equilibrium was indicated by C0. More information on the reaction conditions can be found in the experimental section. A range of measurements were made in order to compare the photocatalytic performance of the various samples. A blank test (MB without any catalyst) was found to have very little photolysis. Figure 7 shows that for the aqueous solution, the absorption intensity progressively dropped as the irradiation time rose.

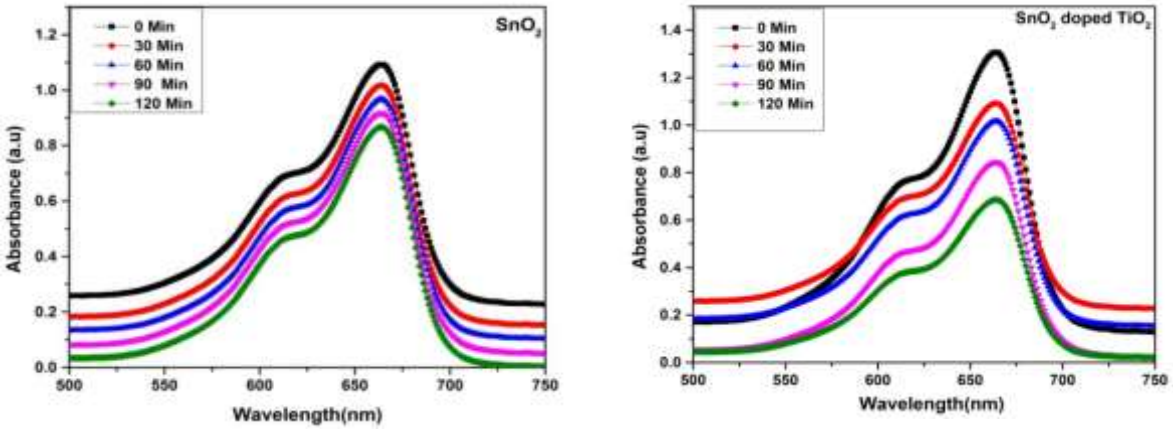

Fig. 7. MB absorption spectra at different times of irradiation in presence of pure and SnO2 doped TiO2 nanoparticles.

The charts showing the variations in concentration (C/C0) for each produced photocatalyst are shown in Fig. 7. The purpose of these plots is to compare the photocatalytic degradation performance of two distinct samples. Degradation efficiencies of 78%, and 94%, for pure SnO2 and SnO2 doped TiO2 nanocomposite samples, respectively, are reported. During 120 minutes of visible irradiation, the SnO2 doped TiO2 nanocomposite photocatalyst shows the best degrading efficiency (94%) when compared to pure SnO2 NPs (78%). There are two reasons for this outstanding outcome. The first benefit is that the doped nanocomposite's effective heterojunction between SnO2 and TiO2 encourages the separation of electron/hole pairs at their contact. To achieve high activity, it is thought that this effective separation of photogenerated electron/hole pairs is essential. Second, the greater specific surface area of the SnO2 doped TiO2 nanocomposite catalyst, which offers more active sites for the adsorption of MB dye molecules and therefore more efficient photocatalytic process, is responsible for the catalyst's better photocatalytic activity. Nevertheless, the dye degradation efficiency (94%), which is achieved by increasing the amount of SnO2 in the doped TiO2 nanocomposite, decreases. This is explained by the fact that a larger concentration of TiO2 in the final composite has the dual effects of shielding the active sites and reducing light absorption. To summarise, the samples' photocatalytic activity can be arranged in the following order: both SnO2 and pure SnO2.

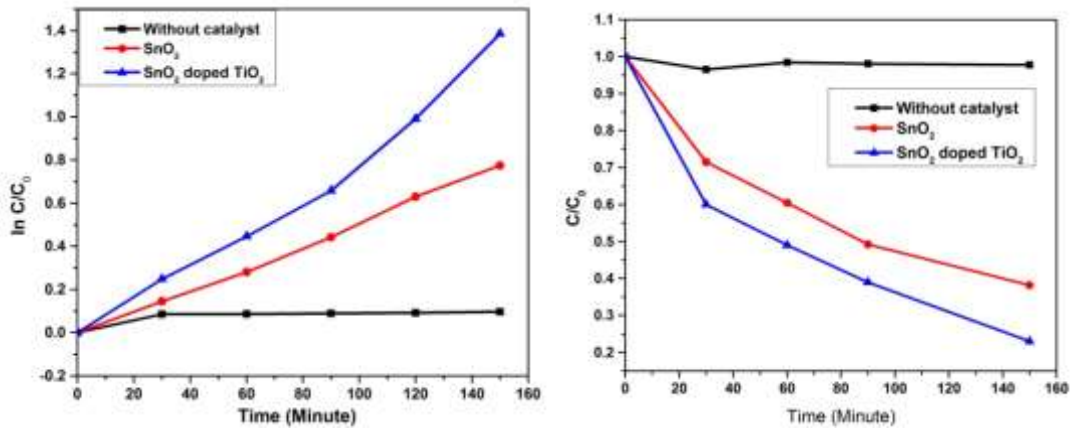

Fig. 8. Plot of degradation efficiency lan C/C0 and C/C0 versus irradiation time for photocatalytic degradation of SnO2@TiO2 nanocomposites

The degrading reaction's pseudo first order kinetics were the main focus of the inquiry. As Figure 8 illustrates, a linear relationship was found between the irradiation time (t) and the plot's slope. The pseudo first order equation model, ln (C0/Ct) = - kt, which denotes the beginning concentration (at 0 min), the concentration, and the rate constant, k, describes the degradation process of the MB dye. The pseudo first order kinetics described the consistent behavior of all the photocatalytic degradation curves. The produced photocatalysts were evaluated using slope fitting lines and degradation rate constants, as shown in Figure 9. The SnO2@TiO2 nanocomposite photocatalyst outperformed the pure SnO2 nanocomposite in terms of degradation efficiency among these parameters.

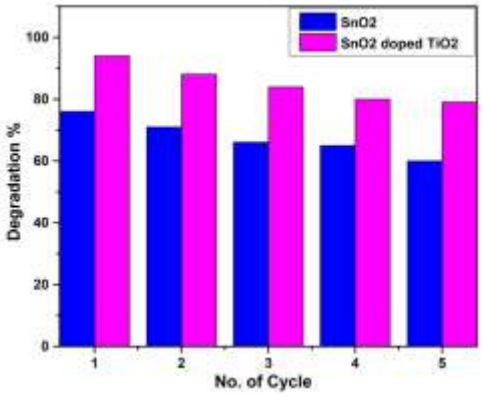

Fig. 8. Plot of degradation efficiency lan C/C0 and C/C0 versus irradiation time for photocatalytic degradation of SnO2@TiO2 nanocomposites

The degrading reaction's pseudo first order kinetics were the main focus of the inquiry. As Figure 8 illustrates, a linear relationship was found between the irradiation time (t) and the plot's slope. The pseudo first order equation model, ln (C0/Ct) = - kt, which denotes the beginning concentration (at 0 min), the concentration, and the rate constant, k, describes the degradation process of the MB dye. The pseudo first order kinetics described the consistent behavior of all the photocatalytic degradation curves. The produced photocatalysts were evaluated using slope fitting lines and degradation rate constants, as shown in Figure 9. The SnO2@TiO2 nanocomposite photocatalyst outperformed the pure SnO2 nanocomposite in terms of degradation efficiency among these parameters.

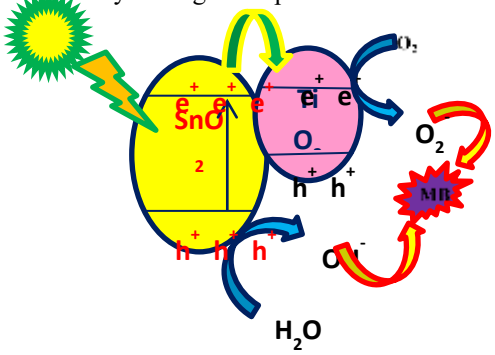

Fig. 10. Photocatalytic mechanism of MB dyes using a visible light catalyst of pure and SnO2doped TiO2 nanocomposite

3.7. Cyclic Voltammetry (CV) analysis

A potential class of materials known as tin oxide (SnO_2) doped titanium dioxide (TiO_2) nanoparticles combines the advantages of SnO_2 and TiO_2, resulting in improved electrochemical, catalytic, and photocatalytic performance. Improved charge transfer characteristics, stability, and overall electrochemical performance can result from doping SnO_2 into TiO_2, which can drastically change the material's electrical structure, surface area, and reactivity. Because of this, SnO_2-doped TiO_2 nanoparticles are excellent choices for use in sensors, catalysis, and energy storage devices like lithium-ion batteries and supercapacitors. Two crucial electrochemical methods for examining the electrochemical characteristics and functionality of SnO_2-doped TiO_2 nanoparticles are cyclic voltammetry (CV) and electrochemical impedance spectroscopy (EIS). By sweeping the potential of a working electrode, cyclic voltammetry (CV) is utilised to assess the electrochemical behaviour of SnO_2-doped TiO_2 nanoparticles over a defined range and measuring the resulting current response. The form and location of the peaks in the CV curve, as seen in Fig. 11, reveal information on the material's electrochemical stability, reaction kinetics, and redox characteristics. The electrochemical potential window in which the material functions is shown by the location of the oxidation and reduction peaks in the CV curve. A more effective electrochemical process is suggested by a smaller potential window and a greater peak current. Due to its high electrical conductivity and capacity to enable charge transfer, SnO_2 doping may improve TiO_2's conductivity and charge transfer capabilities. To evaluate the cycling stability of SnO_2-doped TiO_2 nanoparticles, repeated CV scans are helpful. The material is stable and can preserve its properties if the current response is constant over a number of cycles without experiencing noticeable degradation. its electrochemical properties during use. A decrease in peak current or a shift in peak position over multiple cycles might suggest that the material undergoes structural changes or degradation during cycling.CV analysis of SnO_2-doped TiO_2 nanoparticles is essential for evaluating their potential as electrode materials in lithium-ion batteries, supercapacitors, and other energy storage systems.The redox behavior of SnO_2-doped TiO_2 nanoparticles makes them potential candidates for catalytic applications such as fuel cells, oxygen reduction reactions (ORR), and hydrogen evolution reactions (HER).CV can be used to investigate the sensitivity and selectivity of SnO_2-doped TiO_2 nanoparticles in sensing applications, especially in detecting gases or biomolecules.

Electrochemical Impedance Spectroscopy (EIS) Analysis

One method for examining the impedance response of SnO_2-doped TiO_2 nanoparticles across a frequency range is electrochemical impedance spectroscopy, or EIS. Understanding the entire performance of energy storage and catalytic devices requires knowledge of the material's electrochemical processes, such as charge transfer resistance, ion diffusion, and double-layer capacitance, which are all provided by the data gathered by EIS. The charge transfer resistance (Rct) and the material's electrochemical behaviour can be thoroughly examined using the Nyquist plot, which compares imaginary and real impedance. The charge transfer resistance is represented by a semicircular arc in the high-frequency region of the Nyquist plot, as seen in Fig. 12, the diameter of this arc shows the value of Rct. More efficient charge transfer is suggested by a smaller semicircle in the Nyquist plot, which denotes reduced charge transfer resistance. It is anticipated that doping SnO_2 into TiO_2 will lower the total Rct, improving conductivity and electron mobility. An important metric for assessing the material's electrochemical performance is the charge transfer resistance. In devices like batteries and supercapacitors, a low Rct means that electrons can move between the electrode and electrolyte more readily, improving performance. Due to SnO_2's enhanced conductivity, which serves as a conductive enhancer in the composite, SnO_2-doped TiO_2 nanoparticles should have a lower Rct than pure TiO_2 nanoparticles. The mass transport resistance, which represents the electrolyte's barrier to ion diffusion close to the electrode surface, can be observed from the low-frequency behavior in the Nyquist plot. Ion diffusion constraints may be present and lower the material's performance if the plot displays a straight line in the low-frequency zone. Due to the improved ion diffusion made possible by SnO_2 doping, SnO_2-doped TiO_2 nanoparticles should exhibit lower Rmt than pure TiO_2. Because EIS can quantify changes in impedance in response to surface contacts, it is also frequently used to assess the effectiveness of SnO_2-doped TiO_2 nanoparticles in corrosion prevention and sensing applications (such as gas sensors). These discoveries give SnO_2-doped TiO_2 nanoparticles attractive options for a variety of uses, such as sensors, energy storage, and catalysis.

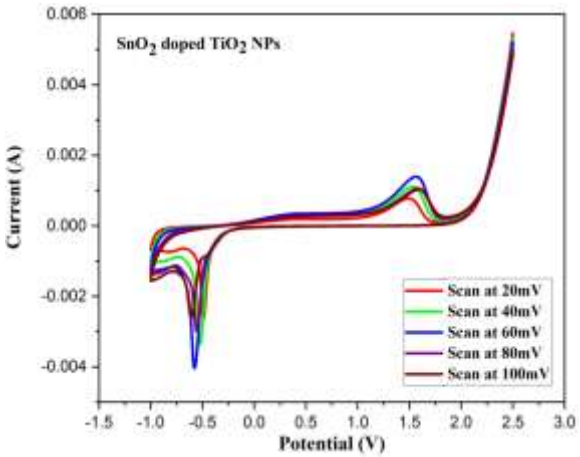

Fig. 11. Cyclic voltametric (CV) plot of SnO2 doped TiO2 nanoparticles

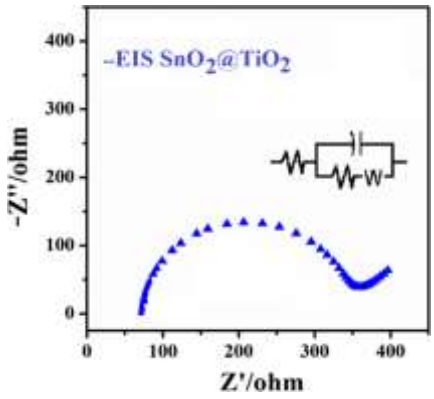

Fig. 12 Electrochemical impedance spectrum (EIS) of SnO2 doped TiO2 nanoparticles

4. CONCLUSION

A simple solution-based method was employed to synthesize the SnO_2-doped TiO_2 nanocomposite. The structural properties and phase formation were confirmed by X-ray diffraction (XRD) and Raman spectroscopy, while transmission electron microscopy (TEM) revealed the successful formation of the SnO_2/TiO_2 heterojunction with well-defined morphology. The photocatalytic performance of the nanocomposite was evaluated using methylene blue (MB) as a model organic pollutant under UV irradiation. The SnO_2-doped TiO_2 nanocomposite exhibited excellent photocatalytic activity, achieving 94% degradation of MB within 120 min, which is significantly higher than that of the individual components. The enhanced degradation efficiency is attributed to the formation of an effective heterojunction that facilitates charge separation and suppresses electron–hole recombination. In addition, the electrochemical properties of the nanocomposite were investigated using cyclic voltammetry (CV) and electrochemical impedance spectroscopy (EIS). The CV results demonstrated improved electrochemical activity, while the EIS analysis revealed reduced charge-transfer resistance, indicating enhanced electrical conductivity and faster interfacial electron transport. These findings confirm that the SnO_2-doped TiO_2 nanocomposite possesses superior photocatalytic and electrochemical performance, making it a promising multifunctional material for environmental remediation and electrochemical energy storage applications.

REFERENCES

1. WK. Kaviyarasu, P.A. Devarajan, S.S.J. Xavier, S.A. Thomas, S. Selvakumar, One pot synthesis and characterization of cesium doped SnO2 nanocrystals via a hydrothermal process, Journal of Materials Science & Technology 28 (1), (2012), 15-20.
2. V. Perumal, C. Inmozhi, R. Uthrakumar, R. Robert, M. Chandrasekar, S. Beer Mohamed, Shehla Honey, A. Raja, Fahd A. Al-Mekhlafi, K. Kaviyarasu, Enhancing the photocatalytic performance of surface - Treated SnO2 hierarchical nanorods against methylene blue dye under solar irradiation and biological degradation, Environmental Research, 209, (2022), 112821.
3. K. Kasinathan, J. Kennedy, M. Elayaperumal, M. Henini, M. Malik, Photodegradation of organic pollutants RhB dye using UV simulated sunlight on ceria based TiO2 nanomaterials for antibacterial applications, Scientific reports 6 (1), (2016), 1-12.
4. M. Chandrasekar, S. Panimalar, R. Uthrakumar, M. Kumar, M.E. Raja Saravanan, G. Gobi P. Madheswaran, C. Inmozhi, K. Kaviyarasu, Preparation and characterization studies of pure and Li+ doped ZnO nanoparticles for optoelectronic applications, Materials Today: Proceedings, 36, (2021), 228-231.
5. M.V. Arularasu, M. Anbarasu, S. Poovaragan, R. Sundaram, K. Kanimozhi, C. Maria Magdalane, K. Kaviyarasu, F.T. Thema, Douglas Letsholathebe, Genene T. Mola, M. Maaza, Structural, optical, morphological, and microbial studies on SnO2 nanoparticles prepared by co-precipitation method, Journal of nanoscience and nanotechnology 18 (5), (2018), 3511-3517.
6. S. Panimalar, R. Uthrakumar, E. Tamil Selvi, P. Gomathy, C. Inmozhi, K. Kaviyarasu, J. Kennedy, Studies of MnO2/g-C3N4 hetrostructure efficient of visible light photocatalyst for pollutants degradation by sol-gel technique, Surfaces and Interfaces 20, (2020) 100512.
7. Amal George, D. MagimaiAntoni Raj, X. Venci, A. Dhayal Raj, A. Albert Irudayaraj, R.L. Josephine, S. John Sundaram, Amal A. Al-Mohaimeed, Dunia A. Al Farraj, Tse-Wei Chen, K. Kaviyarasu, Photocatalytic effect of CuO nanoparticles flower-like 3D nanostructures under visible light irradiation with the degradation of methylene blue (MB) dye for environmental application, Environmental Research, 203, (2022), 111880.
8. N. Geetha, S. Sivaranjani, A. Ayeshamariam, M. Siva Bharathy, S. Nivetha, K. Kaviyarasu, M. Jayachandran, High performance photo-catalyst based on nanosizedZnO - TiO2 nanoplatelets for removal of RhB under visible light irradiation, Journal of Advanced Microscopy Research 13 (1), (2018), 12-19.
9. S. Panimalar, S. Logambal, R. Thambidurai, C. Inmozhi, R. Uthrakumar, AzhaguchamyMuthukumaran, Rabab Ahmed Rasheed, Mansour K. Gatasheh, A. Raja, J. Kennedy, K. Kaviyarasu, Effect of Ag doped MnO2 nanostructures suitable for wastewater treatment and other environmental pollutant applications, Environmental Research, 205, (2022), 112560

10. A. Raja, K. Selvakumar, P. Rajasekaran, M. Arunpandian, S. Ashokkumar, K. Kaviyarasu, S. AsathBahadur, M. Swaminathan, Colloids and Surfaces A: Physicochemical and Engineering Aspects, 564, (2019), 23-30.
11. V. Perumal, A. Sabarinathan, M. Chandrasekar, M. Subash, C. Inmozhi, R. Uthrakumar, Abdulgalim B. Isaev, A. Raja, Mohamed S. Elshikh, SaeedahMusaedAlmutairi, K. Kaviyarasu, Hierarchical nanorods of graphene oxide decorated SnO2 with high photocatalytic performance for energy conversion applications, Fuel, 324, (2022), 124599
12. S. Panimalar, M. Chandrasekar. S. Logambal, R. Uthrakumar, C. Inmozhi, Europium-doped MnO2 nanostructures for controlling optical properties and visible light photocatalytic activity, Materials Today: Proceedings, 56, (2022), 3394-3401
13. M. Chandrasekar, M. Subash, V. Perumal, S. Panimalar, S. Aravindan, R. Uthrakumar, C. Inmozhi, Abdulgalim B. Isaev, SudhakarMuniyasamy, A. Raja, K. Kaviyarasu Specific charge separation of Sn doped MgO nanoparticles for photocatalytic activity under UV light irradiation, Separation and Purification Technology, 294, (2022), 121189
14. M. Chandrasekar, M. Subash, S. Logambal, G. Udhayakumar, R. Uthrakumar, C. Inmozhi, Wedad A. Al-Onazi, Amal M. Al-Mohaimeed, Tse-Wei Chen, K. Kanimozhi, Synthesis and characterization studies of pure and Ni doped CuO nanoparticles by hydrothermal method, J. King Saud Uni. – Sci., 34, (3), (2022), 101831,
15. N. Manjula, K. Kaviyarasu, A. Ayeshamariam, G. Selvan, A. Diallo, G. Ramalingam, S.B. Mohamed, D. Letsholathebe, M. Jayachandran, Structural, morphological and methanol sensing properties of jet nebulizer spray pyrolysis effect of TiO2 doped SnO2 thin film for removal of heavy metal ions, Journal of Nanoelectronics and Optoelectronics 13 (10), (2018), 1543-1551.
16. A.M. Amanulla, C.M. Magdalane, S. Saranya, R. Sundaram, K. Kaviyarasu, Selectivity, stability and reproducibility effect of CeM-CeO2 modified PIGE electrode for photoelectrochemical behaviour of energy application, Surfaces and Interfaces 22, (2021) 100835.
17. C. Thirupathy, S.C. Lims, S.J. Sundaram, A.H. Mahmoud, K. Kaviyarasu, Equilibrium synthesis and magnetic properties of BaFe12O19/NiFe2O4 nanocomposite prepared by co precipitation method, Journal of King Saud University-Science 32 (2), (2020), 1612-1618.
18. K. Kayalvizhi, N.M.I. Alhaji, D. Saravanakkumar, S. Beer Mohamed, K. Kaviyarasu, A. Ayeshamariam, Amal M. Al-Mohaimeed, Mohamed RagabAbdelGawwad, Mohamed S. Elshikh, Adsorption of copper and nickel by using sawdust chitosan nanocomposite beads–A kinetic and thermodynamic study, Environmental Research, 203, (2022), 111814.
19. Y. Subbareddy, R. Naresh Kumar, B.K. Sudhakar, K. Rayappa Reddy, Surendra Kumar Martha, K. Kaviyarasu, A facile approach of adsorption of acid blue 9 on aluminium silicate-coated Fuller's Earth - Equilibrium and kinetics studies, Surfaces and Interfaces 19, (2020), 100503.
20. N.M.I. Alhaji, D. Nathiya, K. Kaviyarasu, M. Meshram, A. Ayeshamariam, A comparative study of structural and photocatalytic mechanism of AgGaO2 nanocomposites for equilibrium and kinetics evaluation of adsorption parameters, Surfaces and Interfaces 17, (2019), 100375.
21. A. George, A. Dhayal Raj, A. Albert Irudayaraj, R.L. Josephine, X. Venci, S. John Sundaram, R. Rajakrishnan, P. Kuppusamy, K. Kaviyarasu, Regeneration study of MB in recycling runs over nickel vanadium oxide by solvent extraction for photocatalytic performance for wastewater treatments, Environmental Research, 211, (2022), 112970.
22. A. Kumar, L. Rout, L. S. K. Achary, A. Mohanty, J. Marpally, P. K. Chand, and P. Dash, Design of Binary SnO2-CuO Nanocomposite for Efficient Photocatalytic Degradation of Malachite Green Dye, AIP Conf. Proc. 1724, (2016), 112-119
23. R. Abinaya, J. Archana, S. Harish, M. Navaneethan, S. Ponnusamy, C. Muthamizhchelvan, M. Shimomura, and Y. Hayakawa, Ultrathin layered MoS2 nanosheets with rich active sites for enhanced visible light photocatalytic activity, RSC Adv. 8, (2018), 26664
24. R. N. Mariammal, K. Ramachandran, B. Renganathan, and D. Sastikumar, On the enhancement of ethanol sensing by CuO modified SnO2 nanoparticles using fiber-optic sensor, Sensors Actuators, B Chem. 169, 199 (2012)
25. M. P. Kumar, G. Murugadoss, R. V. Mangalaraja, and M. R. Kumar, Appl. Phys. A Mater. Enhanced electrocatalytic activity of CuO-SnO2 nanocomposite in alkaline medium, Sci. Process. 127, (2021), 1
26. S. Joshi, S. J. Ippolito, and M. V. Sunkara,Convenient Architectures of Cu2O/SnO2 Type II p-n Heterojunctions and their Application in Visible Light Catalytic Degradation of Rhodamine Blue RSC Adv. 6, (2016), 43672
27. K. Wang, W. Zhang, F. Lou, T. Wei, Z. Qian, and W. Guo, J. Solid State Electrochem. Preparation of electrospunheterostructured hollow SnO2/CuO nanofibers and their enhanced visible light photocatalytic performance 22, (2018), 2413.
28. S. Harish, J. Archana, M. Navaneethan, A. Silambarasan, K. D. Nisha, S. Ponnusamy, C. Muthamizhchelvan, H. Ikeda, D. K. Aswal, and Y. Hayakawa, Enhanced visible light induced photocatalytic activity on the degradation of organic pollutant by SnO nanoparticles decorated hierarchical ZnO nanostructures RSC Adv. 6, (2016), 89721.
29. S. Panimalar, M. Subash, M. Chandrasekar, R. Uthrakumar, C. Inmozhi, Wedad A. Al-Onazi, Amal M. Al-Mohaimeed, Tse-Wei Chen, J. Kennedy, M. Maaza, K. Kaviyarasu, Reproducibility and long-term stability of Sn doped MnO2 nanostructures: Practical photocatalytic systems and wastewater treatment applications, Chemosphere, 293, (2022), 133646.
30. C.M. Magdalane, G.M.A. Priyadharsini, K. Kaviyarasu, A.I. Jothi, G.G. Simiyon, Synthesis and characterization of TiO2 doped cobalt ferrite nanoparticles via microwave method: investigation of photocatalytic performance of Congo red degradation dye, Surfaces and Interfaces, 25, (2021), 101296
31. J. Madona, C. Sridevi, G. Velraj, A. Dhayal Raj, Amal George, Surfactant assisted morphology controlled CuO nanostructures for enhanced photocatalytic performance and bacterial growth inhibition, Materials Science and Engineering: B, 294, (2023), 116562.

32. G. Jayakumar, A. Albert Irudayaraj, A. Dhayal Raj, Photocatalytic Degradation of Methylene Blue by Nickel Oxide Nanoparticles, Materials Today: Proceedings, 4, (2017), 11690-11695,
33. X. Venci, A. George, A. Dhayal Raj, A. Albert Irudayaraj, R.L. Josephine, S. John Sundaram, Self-assembly of CdSe 3D urchins and their photocatalytic response, Environmental Research, 214, (2022), 113804,
34. J. Arumugam, A. Dhayal Raj, A. Albert Irudayaraj, Solvent effects on the properties of Bi2S3 nanoparticles: photocatalytic application, J. Mater. Sci. Mater. in Elect. 28, (2017), 3487–3494.